A human coronavirus OC43-derived polypeptide causes neuropathic pain

Veronica I Shubayev[1,2], Jennifer Dolkas[1,2], Glaucilene Ferreira Catroli[1,2] & Andrei V Chernov[1,2,*]

Abstract

Human coronaviruses have been recently implicated in neurological sequelae by insufficiently understood mechanisms. We here identify an amino acid sequence within the HCoV-OC43 p65-like protein homologous to the evolutionarily conserved motif of myelin basic protein (MBP). Because MBP-derived peptide exposure in the sciatic nerve produces pronociceptive activity in female rodents, we examined whether a synthetic peptide derived from the homologous region of HCoV-OC43 (OC43p) acts by molecular mimicry to promote neuropathic pain. OC43p, but not scrambled peptides, induces mechanical hypersensitivity in rats following intrasciatic injections. Transcriptome analyses of the corresponding spinal cords reveal upregulation of genes and signaling pathways with known nociception-, immune-, and cellular energy-related activities. Affinity capture shows the association of OC43p with an Na^+/K^+-transporting ATPase, providing a potential direct target and mechanistic insight into virus-induced effects on energy homeostasis and the sensory neuraxis. We propose that HCoV-OC43 polypeptides released during infection dysregulate normal nervous system functions through molecular mimicry of MBP, leading to mechanical hypersensitivity. Our findings might provide a new paradigm for virus-induced neuropathic pain.

Introduction

Human coronaviruses (HCoV) causing mild and severe respiratory distress syndromes show evidence for the peripheral and central nervous systems (PNS/CNS) involvement (Burks *et al*, 1980; Talbot *et al*, 1993; Arbour & Talbot, 1998; Arbour *et al*, 1999; Edwards *et al*, 2000; Glass *et al*, 2004; St-Jean *et al*, 2004; Jacomy *et al*, 2006; Dubé *et al*, 2018), potentially contributing to neurological conditions (Boziki *et al*, 2020; Gutiérrez-Ortiz *et al*, 2020; Koralnik & Tyler, 2020; Manji *et al*, 2020; Montalvan *et al*, 2020; Romoli *et al*, 2020; Troyer *et al*, 2020; Ermis *et al*, 2021), including Guillain–Barré syndrome (Kilinc *et al*, 2020; Koralnik & Tyler, 2020; Montalvan *et al*, 2020; Sancho-Saldaña *et al*, 2020; Zhao *et al*, 2020; Koike *et al*, 2021), multiple sclerosis (Burks *et al*, 1980; Cook & Dowling, 1980; Talbot *et al*, 1993; Edwards *et al*, 2000; Boziki *et al*, 2020), and states of neuropathic pain (Kemp *et al*, 2020; Mao *et al*, 2020; Widyadharma *et al*, 2020; Attal *et al*, 2021; McFarland *et al*, 2021; Şahin *et al*, 2021). The virus-mediated pathologies can be accompanied by damage to the myelin sheath of the nervous system and cause rapid-onset demyelination (Croxford *et al*, 2005).

Cationic myelin basic protein (MBP) controls myelin compaction, cytoskeletal interactions, and calcium homeostasis through electrostatic interactions with anionic lipids and proteins (Boggs & Moscarello, 1978; Boggs, 2006). MBP is also a major autoantigen contributing to autoimmune demyelinating disorders, including Guillain–Barré syndrome and multiple sclerosis (Kadlubowski & Hughes, 1979; Musse *et al*, 2006). Molecular mimicry between host and viral proteins (Roos, 1983; Weise & Carnegie, 1988; Adelmann & Linington, 1992; Stohlman & Hinton, 2001; Getts *et al*, 2013), including myelin sheath and HCoV proteins (Wege *et al*, 1983; Talbot *et al*, 2001; Savarin & Bergmann, 2017), are thought to contribute to the etiology of these conditions.

Our earlier work (Kobayashi *et al*, 2008; Kim *et al*, 2012; Liu *et al*, 2012; Ko *et al*, 2016; Shubayev *et al*, 2016, 2018; Hong *et al*, 2017; Chernov *et al*, 2018, 2020; Remacle *et al*, 2018b) implicated immunodominant MBP regions, proteolytically released after PNS damage, in initiating mechanical hypersensitivity through autoreactivity targeted at myelin on mechanosensory neurons. MBP[84–104] peptide injection into an intact sciatic nerve was sufficient to induce sustained pain (Liu *et al*, 2012; Ko *et al*, 2016) via transcriptional reprogramming of metabolic, pronociceptive, and inflammatory signaling in the segmental dorsal root ganglia (DRG) and spinal cord in sex-specific manner (Chernov *et al*, 2020). MBP[84–104] amino acid sequence conservation is critical for its interactions, trafficking, and pronociceptive activity (Chernov *et al*, 2018).

In this report, we identified a coronavirus HCoV-OC43-encoded amino acid sequence with a striking similarity to MBP[84–104]. Past research provided us with biochemical evidence that proprotein convertase furin and/or matrix metalloproteinase (MMP) inflammatory

1 Department of Anesthesiology, University of California San Diego, La Jolla, CA, USA
2 VA San Diego Healthcare System, La Jolla, CA, USA
*Corresponding author. Tel: +1 858 534 1339; E-mail: achernov@ucsd.edu

proteolysis releases cryptic MBP fragments implemented in multiple sclerosis (Shiryaev *et al*, 2009) and PNS injury (Kobayashi *et al*, 2008; Kim *et al*, 2012; Liu *et al*, 2012; Hong *et al*, 2017). We propose that MBP-like polyproteins generated during HCoV infection, similarly, mediate biological activities in PNS/CNS that promote neuropathic pain. Using a synthetic peptide specific to the HCoV-OC43/MBP$^{84-104}$ homologous region, we tested its activity in mechanosensitivity behavior upon sciatic nerve injection followed by RNA-seq, bioinformatics, and proteomic analyses of the unique DRG and spinal cord molecular signatures relative to the scrambled peptide.

Results

Identification of HCoV-OC43 fragment with high amino acid homology to MBP

We have identified the nociceptive activity of the PNS injury-released MBP-derived peptides with highly conserved sequence motifs (Liu *et al*, 2012; Ko *et al*, 2016; Hong *et al*, 2017; Chernov *et al*, 2018). The MBP$^{84-104}$ amino acid sequence, corresponding to positions 84–104 of the human classic MBP isoform 4, was used to search for homologous sequences in public depositories of clinical and environmental coronavirus isolates. Position-specific iterative PSI-BLAST algorithm (www.ncbi.nlm.nih.gov/blast) (Altschul *et al*, 1997; Altschul & Koonin, 1998) was applied with a standard threshold of 0.005. As a result, MBP$^{84-104}$ homologous regions were detected within six individual polyproteins from HCoV-OC43, canine respiratory coronavirus, bovine coronavirus E-AH65, Bat SARS-CoV Rm1/2004 and CoV279/2005, and nucleocapsid protein from porcine epidemic diarrhea (corona)virus (Fig 1A). Because of its relevance to human disease, we selected the amino acid sequence of HCoV-OC43 ORF1ab polyprotein for further analysis. A highly homologous 12 amino acid sequence IVHFFKTFTTST (OC43$^{656-668}$) is localized at positions 656–668 of ORF1ab (at positions 409–421 of p65-like, also known as mouse hepatitis virus (MHV) p65-like protein) (Fig 1B).

Structural similarity revealed by predictive analysis

Although MBP is an intrinsically disordered protein, several regions exhibit secondary structure, including the conserved MBP$^{84-104}$ (Ahmed *et al*, 2012). Predictions conducted with MBP isoform 4 sequence using AlphaFold2 (Jumper *et al*, 2021; Tunyasuvunakool *et al*, 2021) supported these conclusions. Because experimentally resolved 3D structures of HCoV-OC43 p65-like were not available, we predicted structures of both OC43$^{656-668}$ and MBP$^{84-104}$ using Alpha-Fold2 using identical computational parameters. 3D structure models with the highest scores were compared by alignment. A remarkable structural similarity was observed between MBP$^{84-104}$ and OC43$^{656-668}$ (Fig 1C). Each peptide is folded into a characteristic N-terminal α-helix and unstructured C-terminal tail. The aligned α-helices comprised the VHFFK motif, including the invariable histidine-89 (Chernov *et al*, 2018). Less conserved C-terminal tails consisted of multiple threonine/serine residues in close proximity to α-helix. When AlphaFold2 predictions were performed with the full-length proteins (human classic MBP, isoform 4, NP_001020263; HCoV-OC43 p65-like, YP_009555238.1), predicted structures of the corresponding protein

regions and the respective peptides were highly similar. We concluded that OC43$^{656-668}$ exhibited high amino acid sequence homology and structural similarity to the pronociceptive MBP$^{84-104}$ peptide.

HCoV-OC43-derived peptide causes persistent mechanical hypersensitivity in female rats

We have shown repeatedly that MBP$^{84-104}$ peptide produces mechanical allodynia with no effect on thermal sensitivity (Liu *et al*, 2012; Ko *et al*, 2016) likely due to its myelin-dependent pronociceptive activity on myelinated A-afferents, sparing unmyelinated heat-sensitive nociceptors (Shubayev *et al*, 2016). Thus, to test the ability of the OC43-derived peptide to regulate mechanical hypersensitivity characteristics to the homologous MBP$^{84-104}$, we used a synthetic 20-amino acid OC43$^{653-673}$ peptide (OC43p, VSK**IVHFFKTFTTST**ALAFA), and scrambled peptides OC43p-SCR1 and OC43p-S2 designed to mismatch the MBP$^{84-104}$ amino acid sequence. Female rodents display robust mechanical hypersensitivity to intrasciatic MBP$^{84-104}$ relative to males (Chernov *et al*, 2020). Female rats received a single bolus intrasciatic injection (Fig 2A) of OC43$^{653-673}$, scrambled peptides (10 μg in 5 μl, each), or PBS vehicle (5 μl) (*n* = 6/group), followed by von Frey testing. The rats displayed a significant reduction in the mechanical force required to evoke hind paw withdrawal after OC43$^{653-673}$ injection, and the effect was sustained during the 3-week observation period (Fig 2B and C). In contrast, the withdrawal thresholds remained significantly higher in rats injected with OC43p-SCR and alternative OC43p-S2 peptides, or PBS. In agreement, our prior studies found no hypersensitivity arising from scramble MBP$^{84-104}$ peptide sequences and PBS vehicle in the equivalent experimental designs (Liu *et al*, 2012; Ko *et al*, 2016; Hong *et al*, 2017; Chernov *et al*, 2020). No significant contralateral hypersensitivity was observed in response to either peptide. Unstimulated pain-like behavior was measured according to the method described by Attal *et al* (1990) with modifications. Rats injected with OC43p exhibited slightly higher unstimulated pain-like behavioral indices, although differences from the control animals were not statistically significant (Fig 2D). We concluded that OC43p, like MBP$^{84-104}$, induced a robust and sustained pain mechanical hypersensitivity in female rats.

Nerve injections of OC43p induced vast transcriptional changes in the spinal cord

Next, genome-wide transcriptomes were compared in animal groups injected with either OC43p or OC43p-SCR control. Total RNAs from ipsilateral L4–5 DRG and lumbar spinal cord (dorsal quarter) were collected at day 21 post-injection and analyzed by RNA-seq. We detected 17 up- and 21 downregulated differentially expressed genes (DEGs, adjusted *P* (P_{adj}) < 0.1) in DRG in the OC43p group relative to the scrambled-injected group (Fig 3A). In the spinal cord, 724 up- and 160 downregulated DEGs (|Log$_2$(fold change (FC))| > 1, P_{adj} < 0.1) were recorded (Fig 3B, Dataset EV1). The principal component analysis (PCA) (Fig 4A) attributed 87.8% of the variance (PC1) to the effect of peptide injections, highlighting *LOC108348215, Col8a1, Six1, Slc26a7, Kcnj13*, and *Tlr12* genes as the most potent drivers of variation.

Hierarchical clustering (Fig 4B) showed the most significant DEGs ranked by Log$_2$FC between the OC43p and OC43p-SCR groups in the spinal cord. A remarkable enrichment of transcripts encoding many
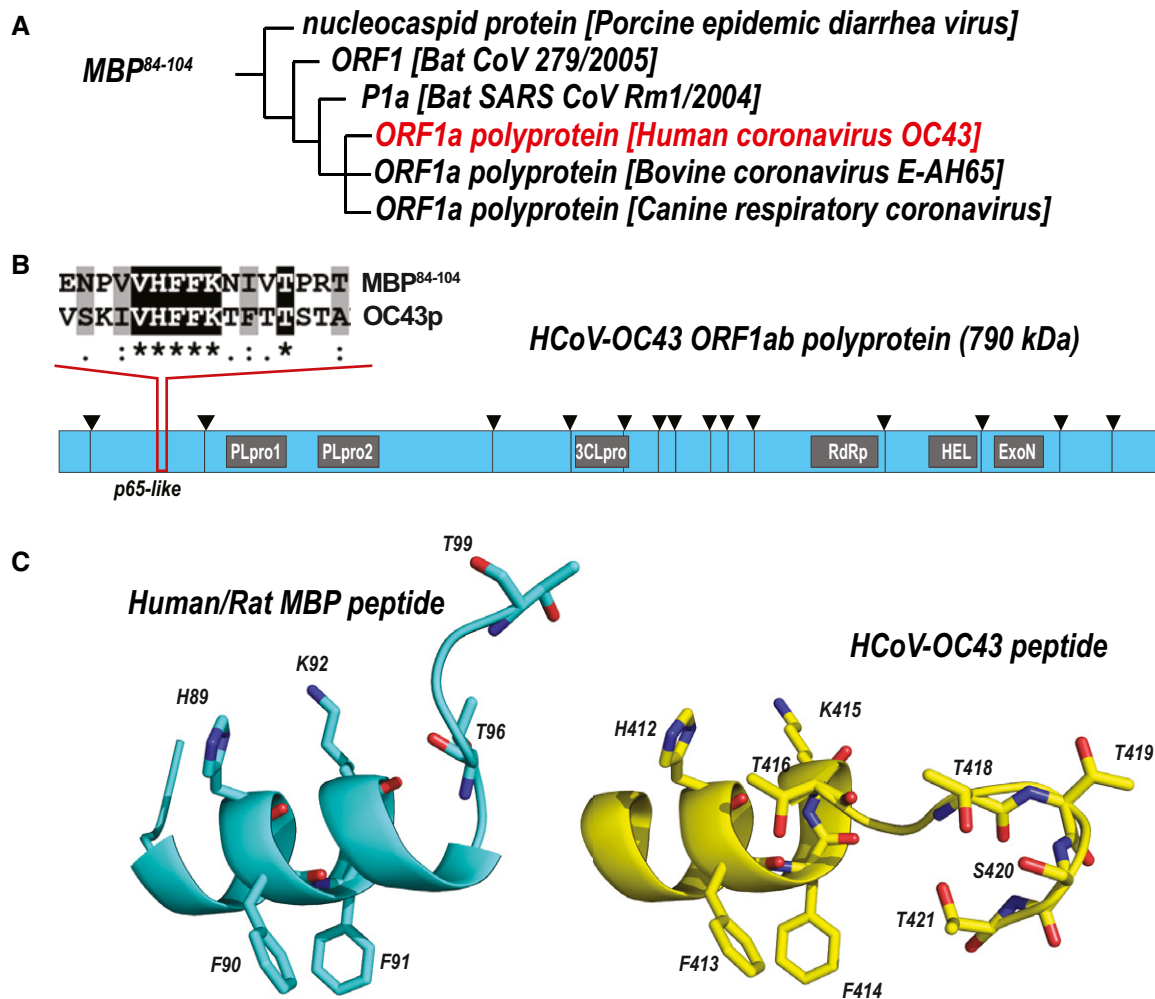
Figure 1. Amino acid sequence homology and structural similarity of OC43p and MBP[84–104].

A MBP[84–104] homology search in Coronaviridae (taxid: 11118) datasets by position-specific iterative (PSI)-BLAST is displayed on a distance tree with a maximum sequence difference of 0.85.

B Schematic organization of HCoV-OC43 coronavirus ORF1ab polyprotein. Triangles indicate the canonical cleavage sites. Amino acid sequence alignment of homologous MBP[84–104] and OC43p is plotted using Clustal Omega.

C 3D structure of MBP[84–104] (blue) and OC43p (yellow) according to AlphaFold2 predictions. Key amino acid residues are labeled by single-letter codes and numbers corresponding to the relative position in the human classic MBP, isoform 4 (NP_001020263), and HCoV-OC43 p65-like (YP_009555238.1). Structures are visualized in PyMOL.

voltage-gated ion channels was observed in the OC43p group. Calcium (*Cacna2d1, Cacnb4, Cacna1c, Cacna1d, Cacng4, Cacna1e, Cacna1a,* and *Cacna1b*) and sodium (*Scn7a, Scn3a, Scn1a,* and *Scn2a*) voltage-gated channels exhibited an increase. A set of potassium voltage-gated channels was upregulated, including *Kcnq3, Kcna3, Kcnj13, Kcnk9, Kcnma1, Kcnh7, Kcnj3,* and *Kcnh5*. Transient receptor channels (*Trpm3, Trps1, Trpc5,* and *Trpm7*), nicotinic receptors (*Chrnb3, Chrna7, Chrna5,* and *Chrnb2*), muscarinic *Chrm2* receptors, glutamate ionotropic NMDA-type receptor *Grin2A*, glutamate ionotropic AMPA-type receptors (*Gria2* and *Gria1),* and GABA receptors (*Gabrg3, Gabra2, Gabra3,* and *Gabrg2*) were significantly upregulated.

Crucial innate immune system genes encoding pattern-recognition receptors (PRPs), including Toll-like receptors (TLRs) *Tlr4, Tlr7, Tlr8, Tlr12,* and *Tlr13*, exhibited upregulation. Interleukin receptors *Il17, Il1, Il20, Il7, Il2,* and *Il6*, and chemokine receptors *Cx3cr* and *Ccr5* increased, although no increase in cytokine ligands was detected.

In female rats, which are susceptible to MBP peptide-induced pain (Chernov *et al*, 2020), we detected a large number of X-linked upregulated DEGs in response to OC43p (Fig 4C). The expression of *LOC100911498* (a homolog of *XIST* non-coding RNA in rats), a marker for Xi in females, exhibited upregulation. Another epigenetic factor crucial for the Xi state, the X-linked chromatin remodeling helicase II (*Atrx*), also demonstrated robust upregulation. Taken together, we concluded that OC43p induced multifaceted transcriptional responses in the PNS/CNS consistent with pronociceptive and proinflammatory signaling.

Gene ontology (GO) analysis identified pronociceptive signaling pathways activated by OC43p

OC43p-regulated signaling pathways were predicted using the Ingenuity Pathway Analysis (IPA) knowledgebase and DEGs with
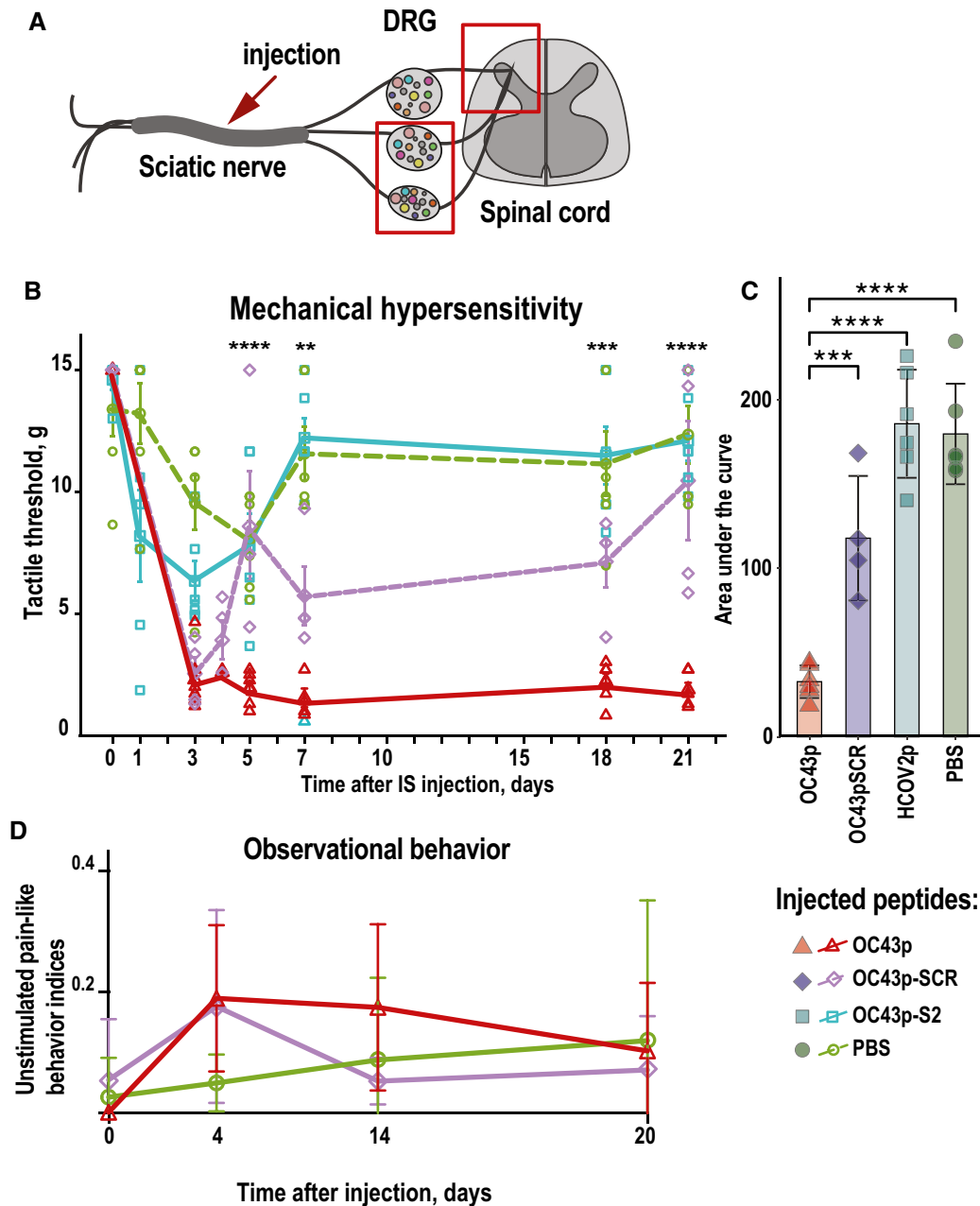
Figure 2. OC43p is a prospective determinant of pronociceptive activity.

A A schematic of the injections into the sciatic nerve followed by ipsilateral DRG and dorsal spinal cord tissue analysis.

B von Frey testing in female rats ($n = 6$/group) at 1–21 days after injections of OC43p peptide, respective control scrambled OC43p-SCR, OC43p-S2 (10 μg in 5 μl, each) peptides, and PBS vehicle. Responses were recorded in ipsilateral hind paws. Mean tactile withdrawal thresholds are in gram force (g) ± standard deviation; two-way analysis of variance (ANOVA) with Bonferroni *post hoc* test: **$P \leq 0.005$; ***$P \leq 0.0005$; and ****$P \leq 0.00005$.

C Areas under the curve (AUC) were calculated for days 1–21 ($n = 6$ animals/group). Bars show the mean AUC and standard deviations (error bars) for each injection group. Data were analyzed by two-way ANOVA with Tukey's *post hoc* test: ***$P \leq 0.0005$; ****$P \leq 0.00005$.

D Observational assays of unstimulated pain-like behavior. Assays were conducted in female rats ($n = 6$/group) after injection of OC43p (red), OC43p-SCR (purple), or PBS (green) on days 4, 14, and 20 post-injection. Each animal was video-recorded for 2 min three times within a 2 h period of time. Hind paw positions were scored to calculate unstimulated pain-like behavioral indices. Index means and standard deviation are shown; two-way ANOVA with Tukey's *post hoc* test was used for group comparisons.

|Log$_2$FC| > 1 and P_{adj} < 0.1. Pathogen response-specific pathways, *FXR/RXR, LXR/RXR, T-cell receptor signaling*, and immune response-specific pathways were affected in DRG (Fig 5A). In the spinal cord,

due to a robust upregulation of multiple voltage- and ligand-gated ion channels, signaling pathways involving neural signal transduction were predictably activated (Fig 5B). Notably, the activation of

A DORSAL ROOT GANGLIA
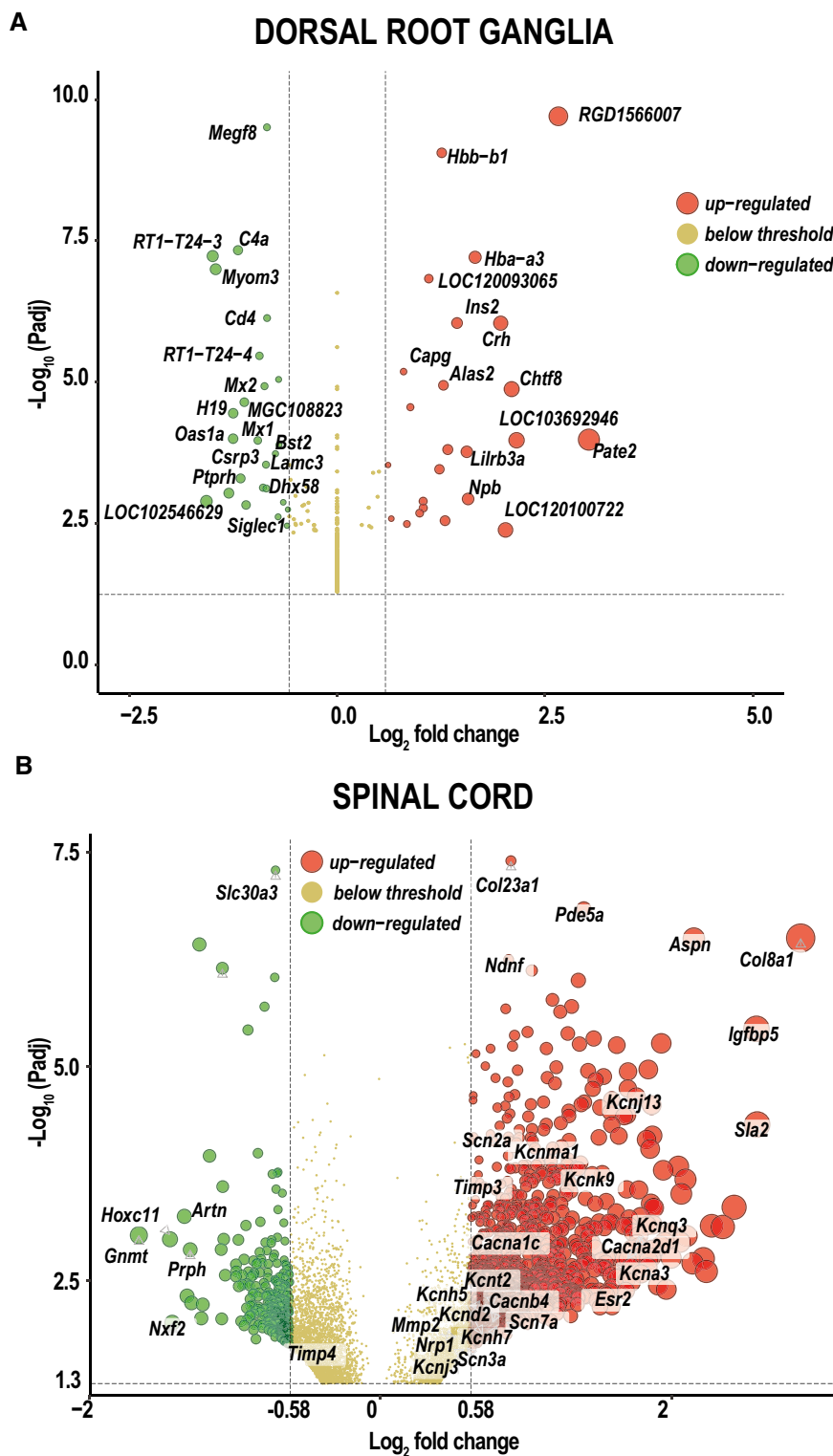
B SPINAL CORD

Figure 3. Transcriptome changes induced by OC43p.

A, B Volcano plots of most significant DEGs in (A) DRG and (B) spinal cord. The size of each circle is proportional to Log$_2$FC. Red and green colors indicate up- and downregulated DEGs, respectively, relative to thresholds (|Log$_2$FC| > 0.58, P_{adj} < 0.1, n = 3/group) displayed by dashed lines. Selected DEGs are labeled.

SPINAL CORD
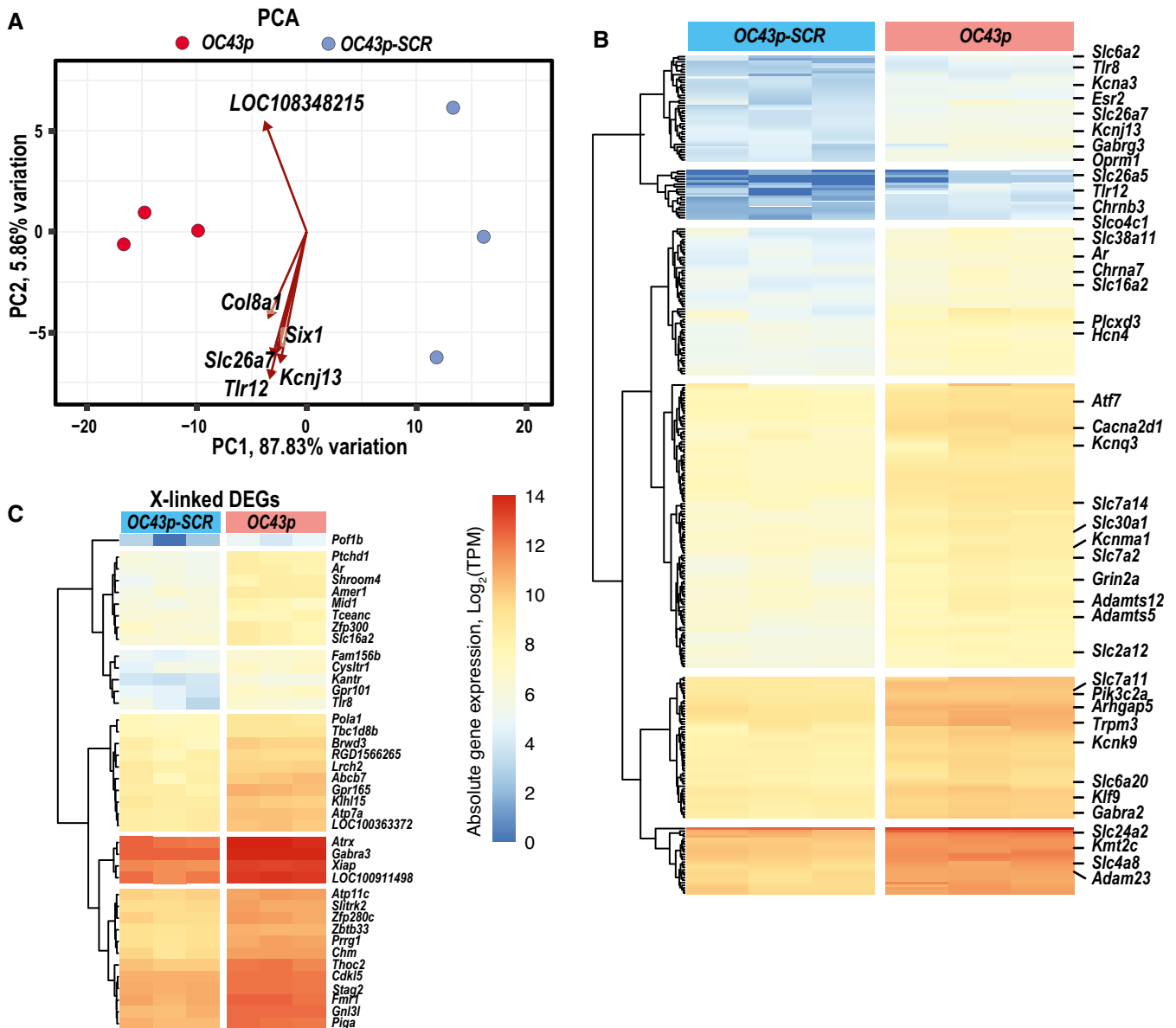
Figure 4. Transcriptome changes in the spinal cord.

A Principal component (PC) analysis of DEGs in OC43p (red) and OC43p-SCR (blue) groups (*n* = 3/group).
B Hierarchical clustering plot of 548 significant upregulated DEGs (Log₂FC > 1, P_{adj} < 0.1, *n* = 3/group). Heatmap color scheme corresponds to logarithms of variance stabilized counts.
C Hierarchical clustering plot of X-linked upregulated DEGs (Log₂FC > 1, P_{adj} < 0.1, *n* = 3/group).

synaptogenesis signaling, CREB signaling in neurons, neuropathic pain signaling in dorsal horn neurons, glutamate receptor signaling, calcium signaling, opioid signaling, and endocannabinoid neuronal synapse pathway was expected in connection with persistent pain hypersensitivity demonstrated by behavioral tests.

The activation of *estrogen receptor signaling and androgen signaling* pathways due to robust *Esr2* and *Ar* upregulation was recorded. The activation of *TLR signaling, neuroinflammation*

signaling pathway, IL-2/IL-6/IL-8, and *PI3K signaling in B lymphocytes* was low to moderate relative to other pathways. It is worth noting the activation of the long-coding RNA *HOTAIR regulatory pathway* was previously not associated with pain signaling. Pathways related to mitochondrial function, metabolic pathways, and protein synthesis demonstrated a decline. Remarkably, *prolactin signaling* was elevated (Fig 5B) due to more than twofold elevation of genes encoding prolactin receptor dimer (Prlp/Prlr), Irs1, potassium
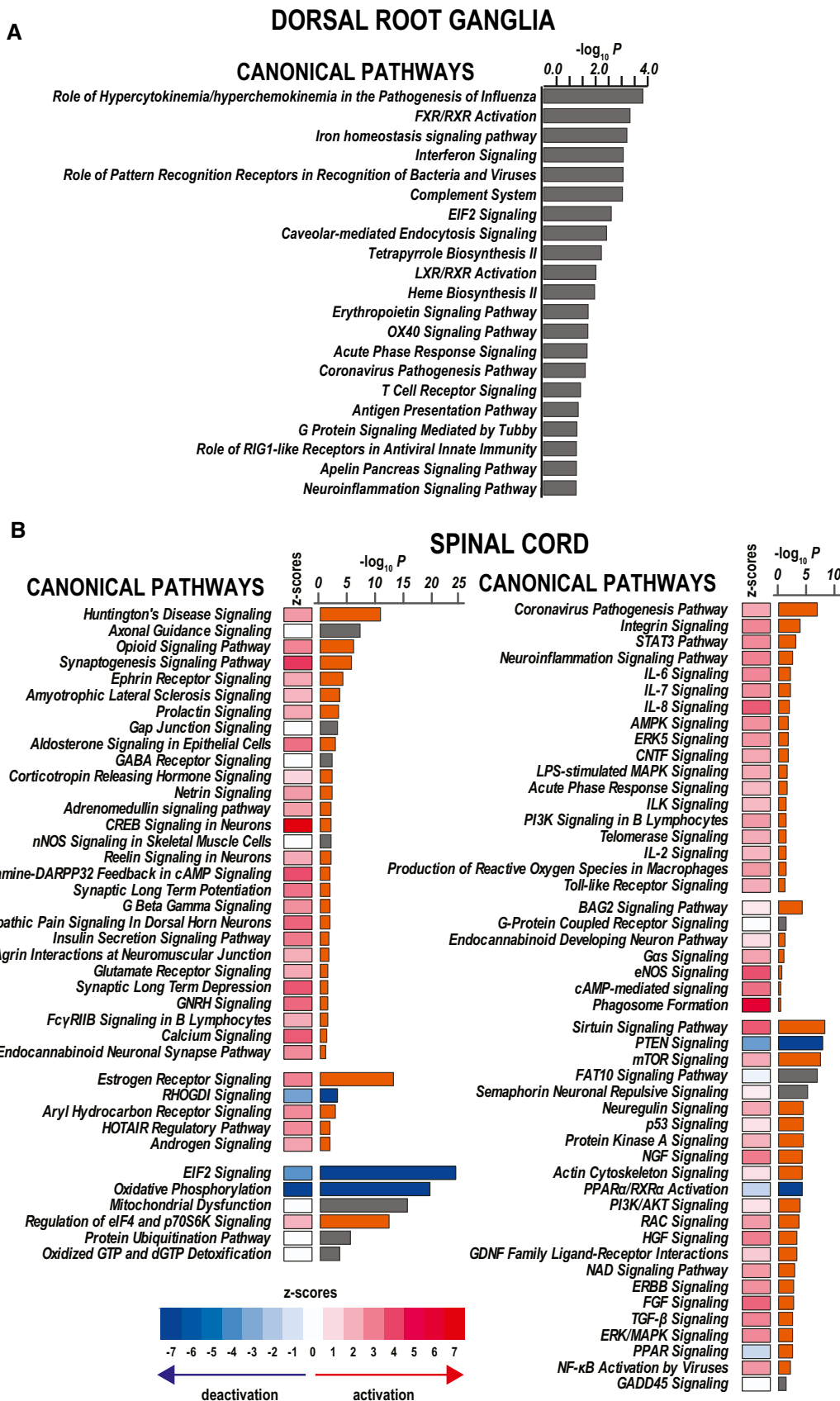
Figure 5.

Figure 5. Canonical pathways affected by OC43p.

A, B Canonical pathways (A, DRG and B, spinal cord) identified by IPA are ranked by P (-$\log_{10}P$). Positive and negative z-scores (in the spinal cord) indicate upregulation or downregulation, respectively, according to the color scale. Bar colors correspond to significant activation (orange), deactivation (blue), or no change (gray) in pathway regulation.

channel Kcnma1, PI3K family member Pik3c2a, protein kinase C epsilon type (PKCε), Irs1, and Socs4 (Fig 6A).

The most significant DEGs were attributed to molecular functions (MFs) using the GO database to enrich the biological interpretation. The best-match average (BMA) distance plot represents the proximity of the eleven MF clusters (Fig 6B) summarized on the distance heatmap (Fig 6C). A broad range of cellular functions was affected, including transcriptional regulation, ribosome activity, binding to fatty acids, hormones, and ECM (collagen and fibronectin). We identified signaling pathways, including voltage-gated ion channel activity, ligand-gated channel activity, and cytokine receptor activity directly relevant to pain hypersensitivity and nociception.

OC43p affinity to the Na$^+$/K$^+$-transporting ATPase complex

To identify proteins potentially interacting with OC43p, we conducted the affinity capture in rat protein lysates (spinal cord) using biotinylated OC43p and OC43p-SCR peptides bound to paramagnetic beads. To reduce non-specific binding, in the protein lysates we preincubated with OC43p-SCR beads. Beads were removed and affinity capture was conducted with OC43p-bound beads. Bound proteins were digested with trypsin, digestion products were separated by liquid chromatography, and analyzed by mass spectrometry. Strikingly, Atp1a1, Atp1a2, Atp1a3, and Atp1b1 proteins produced high significance scores and peptide coverages 32% to 57% (Fig 7A). These proteins represent subunits of the Na$^+$/K$^+$-transporting ATPase complexes (Fig 7B) (http://geneontology.org). According to RNA-seq, the expression of the ATPase subunits is high in the spinal cord and DRG but lower in sciatic nerves (Fig 7C). Protein immunoblotting further confirmed that Atp1a1 and Atp1a2 interaction is specific to OC43p (Fig 7D; Atp1a3 and Atp1b1 were not probed).

Discussion

Neurotropic viruses (Johnson, 1999; Dahm et al, 2016; Maximova et al, 2021), including HCoVs (Burks et al, 1980; Talbot et al, 1993; Arbour & Talbot, 1998; Arbour et al, 1999; Edwards et al, 2000; Glass et al, 2004; St-Jean et al, 2004; Jacomy et al, 2006; Dubé et al, 2018), expose cells to overwhelming quantities of viral proteins and, due to molecular mimicry with host proteins (Roos, 1983; Wege et al, 1983; Weise & Carnegie, 1988; Adelmann & Linington,

1992; Stohlman & Hinton, 2001; Talbot et al, 2001; Getts et al, 2013; Savarin & Bergmann, 2017), may disrupt cellular protein–protein/RNA/DNA/lipids interactions in the host. Expectedly, HCoV sequence evolution continues to introduce novel amino acid sequence patterns, which may eventually include novel HCoV strains, such as SARS-COV-2. Molecular mimicry can assist the virus in hijacking host-specific functions to (i) mediate immune and neuroimmune responses in the upstream, uninfected regions of the nervous system by axonal trafficking; and (ii) directly affect transcriptional programs in the PNS/CNS neurons in favor of virus survival and immune system evasion. Interference with the PNS/CNS regulatory networks leads to detrimental long-term neurological health outcomes (Burks et al, 1980; Cook & Dowling, 1980; Talbot et al, 1993; Edwards et al, 2000; Boziki et al, 2020; Gutiérrez-Ortiz et al, 2020; Kemp et al, 2020; Kilinc et al, 2020; Koralnik & Tyler, 2020; Manji et al, 2020; Mao et al, 2020; Montalvan et al, 2020; Romoli et al, 2020; Sancho-Saldaña et al, 2020; Troyer et al, 2020; Widyadharma et al, 2020; Zhao et al, 2020; Attal et al, 2021; Koike et al, 2021; McFarland et al, 2021).

As a proof of concept, the perspective synthetic peptide used in this study was derived based on strong sequence and structure homology to MBP[84–104]. The OC43/MBP homologous region is localized at positions 407–422 of the MHV p65-like protein of HCoV-OC43 (GenBank ID YP_009555247), and sequences with such identity are unknown in other (corona)viruses to date. The expression and proteolytic processing of this protein product during viral infections as part of the pp1ab polyprotein were demonstrated in cells infected with coronaviruses and related viruses (reviewed in Weiss et al, 1994). We propose that nociceptive activity can be exhibited by polypeptides of varying lengths. Our investigation centers on the MBP homologous sequence accessible for interaction with respective host protein targets. It is noteworthy that peptide epitopes were used in a conceptually similar study that established high-affinity molecular mimicry based on a short amino acid homologous motif shared by the Epstein–Barr virus-encoded transcription factor EBNA1, and host-encoded GlialCAM protein was implicated in multiple scleroses (Lanz et al, 2022). Future translational and clinical studies in patients with diagnosed infections can ascertain the precise identity of the pronociceptive viral polypeptides.

In MBP, the algesic sequence is buried inside the intact protein and becomes exposed for interaction after proteolytic degradation of MBP by cellular peptidases as we shown previously. If the MBP-like viral sequences are readily exposed to the interface of unprocessed

Figure 6. Pronociceptive signaling induced by OC43p in rat spinal cord.

A Prolactin signaling pathway plotted in IPA. Red and green colors indicate up- and downregulated DEGs, respectively, relative to thresholds (|Log$_2$FC | > 0.58, P_{adj} < 0.1). Orange arrows indicate activation of signaling.

B Gene ontology (GO) molecular function clusters are schematically shown on a two-dimensional scaling plot. Cluster groups 1–11 are marked by colors and explained on panel 6C. Clusters of potentially pronociceptive molecular functions are circled.

C Molecular function clusters are summarized on the best-match average (BMA) distance heatmap. Heatmap colors correspond to a number of GO terms in each cluster.
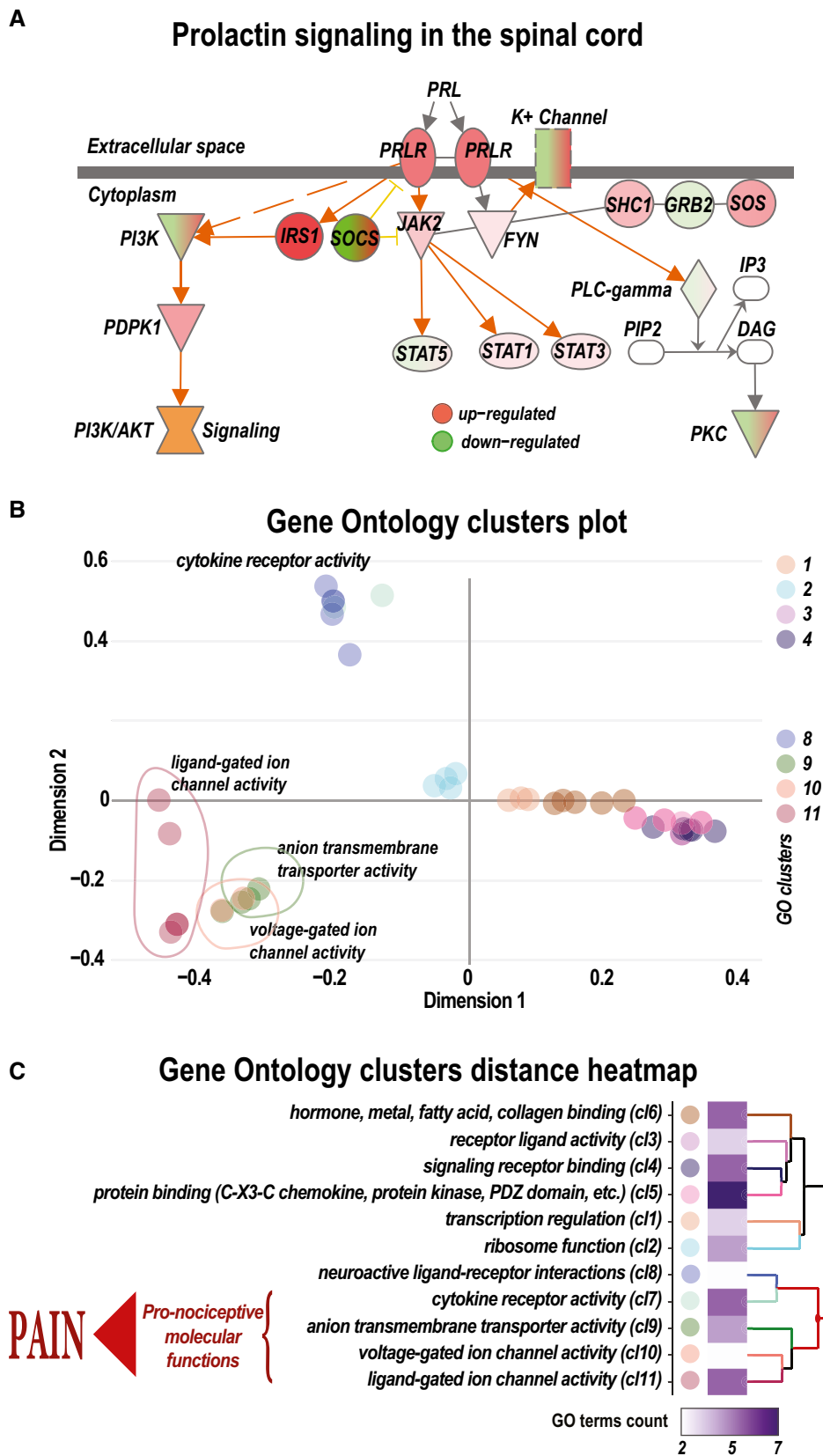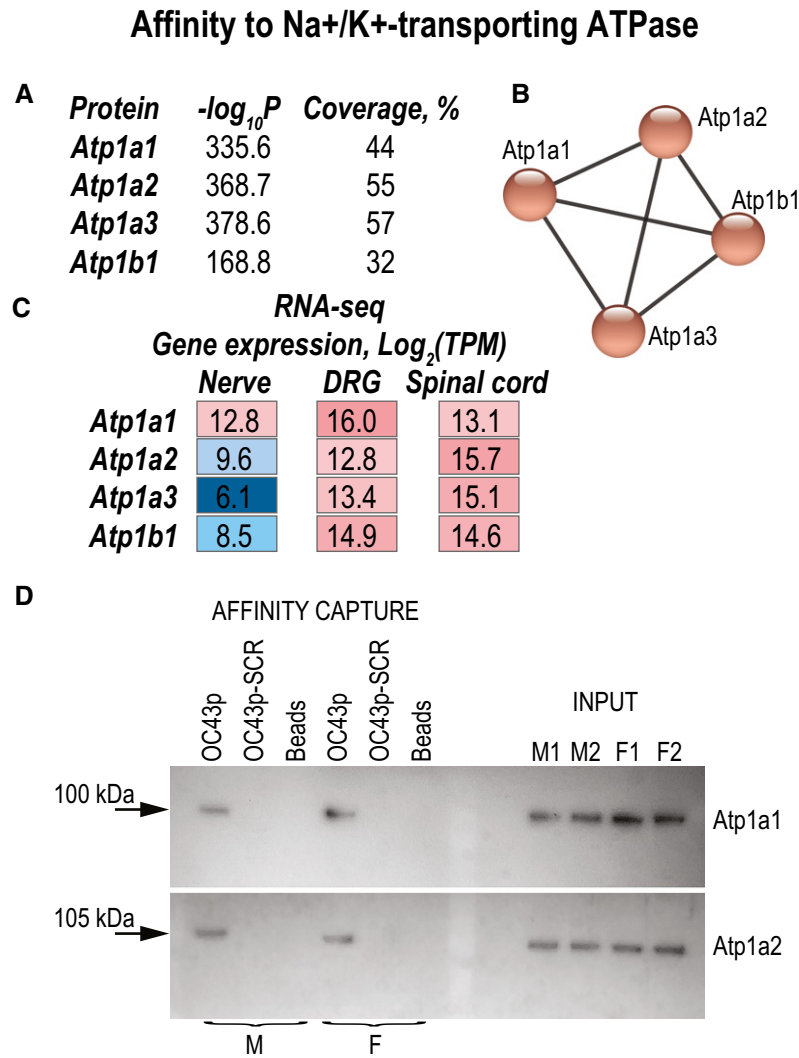
A

Prolactin signaling in the spinal cord

B

Gene Ontology clusters plot

C

Gene Ontology clusters distance heatmap

Figure 6.

Affinity to Na+/K+-transporting ATPase

A

Protein	$-log_{10}P$	Coverage, %
Atp1a1	335.6	44
Atp1a2	368.7	55
Atp1a3	378.6	57
Atp1b1	168.8	32

B

C

RNA-seq
Gene expression, $Log_2(TPM)$

	Nerve	DRG	Spinal cord
Atp1a1	12.8	16.0	13.1
Atp1a2	9.6	12.8	15.7
Atp1a3	6.1	13.4	15.1
Atp1b1	8.5	14.9	14.6

D

Figure 7. OC43p affinity to the Na$^+$/K$^+$-transporting ATPase complex.

A Mass spectrometry identification of the Atp1 family of proteins captured by biotinylated OC43p peptide in rat dorsal spinal cords from female rats ($n = 2$/groups). Negative $log_{10}P$ – confidence score and peptide sequence coverage (%) were calculated in PEAKS Studio™ 8.5 (BSI).

B Relationship of ATPase subunits identified in string-db.org. Lines indicate evidence-based interactions.

C ATPase gene family expression in sciatic nerves, DRG, and spinal cords of naïve rats. TPM (transcripts per kilobase million) measures the transcription frequency of a specific gene by RNA-seq ($n = 3$/group). Blue to red color intensity corresponds to $Log_2(TPM)$.

D Affinity capture of proteins by OC43p- and OC43-SCR-bound magnetic beads. Specific reactivity to Atp1a1 and Atp1a2 was detected by protein immunoblotting using specific primary antibodies. OC43p-SCR-coated and uncoated beads (Beads) were used to control non-specific binding. Spinal cords were isolated from male (M) and female (F) rats ($n = 2$/group). Input protein lysates (right side, in duplicates) served as loading controls. Approximate molecular weights (in kDa) are indicated by arrows.

or partially processed viral proteins, further proteolytic cleavage of the viral polypeptides to shorter peptides is not a prerequisite of molecular mimicry activity. We hypothesize that viral infection-related proteolytic mechanisms, such as the inflammatory proprotein convertase/MMP proteolytic pathway (Shiryaev *et al*, 2009), and viral intrinsic proteinases, can further stimulate a release of cryptic viral peptidic fragments with biological activities. Intriguingly, recent evidence that MMP2/MMP9 can activate the SARS-CoV-2 fusion (preprint: Benlarbi *et al*, 2022) in cells expressing high levels of MMPs provides a connection with the role of these MMPs in nerve injury and pain (Shubayev *et al*, 2006; Chattopadhyay *et al*,

2007; Kobayashi *et al*, 2008; Kim *et al*, 2012; Liu *et al*, 2012; Remacle *et al*, 2015, 2018a).

The N-terminal invariable 87-(V/I)VHFFK-92 motif of MBP$^{84–104}$ and OC43p is folded into structurally similar α-helices. The unstructured C-terminal tails included 3–5 threonine and serine residues, subject to enzymatic phosphorylation by MAPK, CDK5, GSK3 (Pelech, 1995; Chernov *et al*, 2018), and other kinases. Dynamic phosphorylation/dephosphorylation by cellular kinases can engage a regulatory switch critical for the peptide's biological activity. We propose that the bipartite characteristics of the MBP$^{84–104}$ and OC43p peptides may be crucial to promoting pronociceptive and

other neuropathological activity. We identified an intriguing affinity of OC43p to the Na⁺/K⁺-transporting ATPase complex responsible for electrochemical cation gradient across the plasma membrane and electrical excitability in the nervous system. The ATPase's multiple subunits have been implicated in Charcot–Marie–Tooth disease, peripheral neuropathies, neuromuscular disorders (reviewed in Clausen *et al*, 2017), and inflammation-induced mechanical allodynia (Wang *et al*, 2015). In the context of virus–host interaction, based on our transcriptomics analysis and affinity capture assay we hypothesize that OC43p can directly affect ion transport and aberrant neuroplasticity leading to persistent mechanical allodynia.

We demonstrated that OC43p induced persistent pain hypersensitivity in female rats. Females are more susceptible to developing chronic pain states as compared to males, including MBP-induced pain in rodents (Chernov *et al*, 2020). Bioinformatics analysis of RNA-seq data illuminated pronociceptive transcriptional changes in the dorsal spinal cord established within three weeks after sciatic nerve injection. Supporting the observed pain effects, peripheral terminals of nociceptor neurons and spinal higher-order neurons in the dorsal spinal cord increased expression of a broad spectrum of ion channels in response to OC43p. This observation was consistent with its potential role in neuron excitability in the pain sensation (Suzuki & Dickenson, 2000; Julius & Basbaum, 2001; Kidd & Urban, 2001). Our prior observations of mechanical hypersensitivity were not accompanied by thermal hyperalgesia in response to the homologous MBP[84–104] peptide (Liu *et al*, 2012; Ko *et al*, 2016) consistent with the model of a myelin-dependent pronociceptive activity on myelinated A-afferents, sparing unmyelinated heat-sensitive nociceptors (Shubayev *et al*, 2016).

The proallodynic MBP[84–104] activity and the downstream signaling are sexually dimorphic (Chernov *et al*, 2020). In agreement, upregulation of sex hormone receptors *Esr2* and *Ar* in females in response to OC43p predicts activation of the estrogen and androgen signaling pathways, respectively, and potentially virus-induced hypersensitivity. Upregulated cytokine receptor genes and respective signaling pathways outlined the mechanistic link between *Esr2*, neuroimmune properties of glia, and neuronal excitability as a characteristic of sustained neuropathic states. Accordingly, activation of prolactin signaling (Patil *et al*, 2019) and the regulatory role of the X chromosome in immunity, (neuro)-inflammation, and neuropathic pain (Syrett *et al*, 2019; Shenoda *et al*, 2021; Tang *et al*, 2021) contributed to the female-specific pain response. Accordingly, we observed unexpected upregulation of the *XIST* homolog and other X-linked epigenetic factors. The role of sexual dimorphism in coronavirus-related chronic pain requires focused investigation using both female and male animals.

To summarize, our data strongly support the pronociceptive biological activity of OC43p due to molecular mimicry mechanisms to a neural-specific host protein, MBP. We propose that HCoVs evolve their encoded protein sequences to mimic host proteins in order to hijack cellular programs related to immune, metabolic, and cellular energy functions in the somatosensory nervous system. The HCoV peptide's identification in clinical specimens, their pronociceptive properties, and pathobiochemical processes of their release constitute topics of perspective research.

Materials and Methods

Peptides

Peptides OC43p (VSKIVHFFKTFTTSTALAFA), OC43p-SCR (VFIAHSVKFTKSFTLATTFA), and OC43p-S2 (DNPVLHYFASTEKSN) were synthesized with > 95% purity, N-terminal acetyl, and C-terminal amide groups. Trifluoroacetic acid was removed after synthesis, and counterions were exchanged for acetates. Biotin-tagged peptides were synthesized with N-terminal biotin modifications. Peptides were dissolved in sterile PBS (vehicle). Key reagents and resources are described in Table EV1.

Antibodies

Antibodies used for protein immunoblotting were as follows: anti-Na⁺/K⁺-transporting ATPase α-1 antibody, clone C464.6 ZooMAb® mouse monoclonal IgG (Millipore Sigma, Cat. no. ZMS1029, used at 1:5,000 dilution); rabbit polyclonal anti-Na⁺/K⁺-transporting ATPase α-2 antibody (Millipore Sigma, Cat. no. 07-674, at 1:2,500 dilution); cross-adsorbed donkey anti-rabbit, horseradish peroxidase (HRP)-conjugate (Thermo Fisher, Cat. no. 0031458, at 1:5,000 dilution); and goat anti-mouse IgG (H + L) HRP-conjugate (Bio-Rad, Cat. no. 1706516, at 1:5,000 dilution).

Amino acid homology search

Amino acid sequence homology search was conducted using position-specific iterative PSI-BLAST tool (www.ncbi.nlm.nih.gov/blast) (Altschul *et al*, 1997; Altschul & Koonin, 1998) within NCBI (www.ncbi.nlm.nih.gov), VIPR (www.viprbrc.org), and GISAID SARS-CoV-2 mutant variants (www.gisaid.org) depositories.

Protein structure predictions

AlphaFold2 (Jumper *et al*, 2021) in ColabFold (preprint: Mirdita *et al*, 2021) with multiple sequence alignments generated by MMseqs2 was used to predict 3D structure. Predicted models were aligned, processed, and visualized in PyMOL (www.pymol.org).

Animal procedures

Sprague Dawley female rats (8–10 weeks old) were obtained from Envigo and housed in a temperature-controlled room (~22°C), on a 12-h light/dark cycle, and with free access to food and water. All procedures were conducted during the daytime. Under isoflurane anesthesia, the common sciatic nerve was exposed unilaterally at the mid-thigh level. A single bolus injection of the peptides (10 µg in 5 µl vehicle) into a nerve fascicle was performed using a 33-gauge needle on a Hamilton syringe. All animal procedures were performed according to the Policy on Humane Care and Use of Laboratory Animals and the protocol approved by the Institutional Animal Care and Use Committee at the VA San Diego Healthcare System. Weekly weight measurements and daily assessments of the hydration status and post-operative wound infection were conducted. Animals that developed surgery-related abnormalities were excluded from the study.

Behavioral tests

All behavioral measurements were taken by a tester blinded to the experimental groups. Animal groups were formed randomly. von Frey testing was performed before and at the indicated time points after peptide injections ($n = 6$/group). Rats were placed in individual compartments with a wire mesh bottom. von Frey filaments (0.41–15.2 g, Stoelting) were applied perpendicularly to the mid-hind paw for 4–6 s. A withdrawal response was recorded by an experimenter blinded to the groups. The 50% probability of withdrawal threshold was determined by up-down method as described previously (Chernov *et al*, 2020) using software developed in R (https://github.com/chernov-lab/VonFreyTest). Areas under the curve were calculated using Prism 9 (GraphPad).

Unstimulated pain-like behavior was analyzed on days 4, 14, and 20 post-injection as previously described (Attal *et al*, 1990; Paulson *et al*, 2002; Chattopadhyay *et al*, 2007) with modifications. Each animal was video-recorded for 2 min three times within a 2 h period of time. Positions of the injected hind paw were continuously rated according to the scoring system: 0, the paw was placed normally on the floor; 1, the paw was placed lightly on the floor, and the toes were in a ventroflexed position; 2, only the inner edge of the paw was placed on the floor; 3, only the heel was placed on the floor, and the hind paw was inverted; 4, the hind paw was elevated; and 5, animal licked the hind paw. Scoring data were interpreted using custom Java software. Unstimulated pain-like behavioral indices were calculated by the time interval the rat spent in each behavior multiplied by weighting factors, and divided by the length of the observational period according to the formula:

$$\text{index} = \frac{0 \cdot t_0 + 1 \cdot t_1 + 2 \cdot t_2 + 3 \cdot t_3 + 4 \cdot t_4 + 5 \cdot t_5}{120}$$

where t_0–t_5 is the time duration (s).

Samples

Tissues (DRG and spinal cord, lumbar (L)1–6, quartered) were placed in 500 μl RNAlater, left at 4°C overnight, and then stored at −20°C. All sample groups were processed synchronously to minimize batch effects.

RNA purification

Tissues were homogenized, and total RNAs were purified using RNeasy reagents. RNA concentration and integrity were determined using Qubit 4 and Bioanalyzer, respectively. 500 ng of RNA (3 replicates/group) with RIN ≥ 7.0 was used for RNA-seq.

RNA-seq

RNA-seq library preparations and sequencing were performed at the Genomics High Throughput Facility (University of California, Irvine). In brief, mRNA libraries were generated following the TruSeq Stranded mRNA library preparation protocol (Illumina). Poly-A-enriched mRNAs were purified using poly-T oligo coupled magnetic beads, followed by mRNA fragmentation, first and second strands synthesis, cleaning on AMPure XP beads, and 3'-adenylation. Ligation of TruSeq dual-index adapters was used for barcoding. The quality of RNA-seq libraries was validated using qPCR. Libraries were sized on an Agilent Bioanalyzer DNA high-sensitivity chip and normalized. RNA-seq was performed using the paired-end 100 cycle program on the NovaSeq 6000 system. Base calls were recorded and converted to FASTQ files containing sequencing reads and the corresponding quality scores using Illumina software. Sequencing was conducted until at least 25 million paired-end reads per sample were acquired.

Data processing

The data analysis workflow is schematically presented in Fig EV1. FASTQ files were filtered to remove low-quality bases, TruSeq dual-index adapter sequences, and unpaired reads using Trimmomatic (Bolger *et al*, 2014). Transcript-level quantification was performed using Salmon (Patro *et al*, 2017) in quasi-mapping mode using the Rat genome version R7. To correct systematic biases commonly present in RNA-seq data, *-seqBias* and *-gcBias* options were applied. Transcript- to gene-level conversion was done using Tximeta (Love *et al*, 2020). RNA-seq coverage and data quality were assessed using MultiQC (Ewels *et al*, 2016).

Gene count matrices were imported into the DESeq2 package (Love *et al*, 2014). Outliers were identified by Cook's distance method and excluded from further analysis. Dataset's normalization was conducted using trimmed M-values (TMM) included in the DESeq2 package. Log$_2$FC was calculated using the Wald test. The adjusted (shrunken) Log$_2$FC values were calculated using the adaptive t-prior apeglm method (Zhu *et al*, 2019). Significant DEGs were identified by P_{adj} values below a false discovery rate cutoff ($P_{adj} < 0.05$) (Dataset EV1). $P_{adj} < 0.05$ was used in downstream analyses unless otherwise noted. Batch effects were controlled using removeBatchEffect (Ritchie *et al*, 2015) and RUVseq (Risso *et al*, 2014) functions.

Signaling pathway analysis

Bioinformatics tools used for the processing of RNA-seq data are listed in Table EV1. Ingenuity Pathway Analysis based on the causal network approach (Krämer *et al*, 2014) was used to predict signaling pathway regulation. The activation directionality was estimated based on z-scores. Gene ontology analysis was performed using ViSEAGO package and other Bioconductor tools.

Affinity capture assay

Peptide-bound beads were prepared by incubating biotin-tagged OC43p and OC43p-SCR peptides (9 nmole) with 100 μl Dynabeads MyOne Streptavidin T1 (10 mg/ml) for 2 h at 25°C in 500 μl of TBST (20 mM Tris, 150 mM NaCl, 0.1% Tween-20, and pH 7.4). Beads were washed using a magnetic separation rack 6 times with 750 μl TBST to remove unbound peptides, and resuspended in 100 μl of affinity capture buffer (TBST supplemented with 1 mM CaCl$_2$, 1 mM MgCl$_2$, 1 mM Na$_3$VO$_4$, and EDTA-free protease inhibitors (Roche)).

All affinity capture steps were performed at 4°C. Frozen rat dorsal spinal cord tissues were submerged in 300 μl of lysis buffer

(affinity capture buffer supplemented with 50 mM octylthiogluco-side (OTG)), and homogenized using BioMasher microhomogen-izers for 1 min, followed by centrifugation in QiaShredder units (Qiagen) for 5 min at 21,000 *g*. Protein lysates were diluted with affinity capture buffer and pre-adsorbed with 100 μl Dynabeads MyOne Streptavidin T1 (10 mg/ml) for 2 h with agitation. Lysates were incubated overnight with 50 μl of respective peptide-bound beads with agitation. Beads were washed seven times with 750 μl of TBST. For mass spectrometry, beads were washed three times with 750 μl PBS. For immunoblotting, proteins were eluted by heating at 70°C for 10 min in 100 μl of NuPAGE LDS Sample Buffer (Thermo Fisher Scientific) supplemented with 50 mM 1,4-dithiothreitol. Protein concentrations were measured using a bicinchoninic acid assay.

Liquid chromatography and mass spectrometry

LC/MS was performed at the Biomolecular Mass Spectrometry Facil-ity (University of California San Diego). In brief, affinity-captured proteins were trypsin-digested, and peptides were separated by liq-uid chromatography for 1.5 h using a reverse-phase C18 gradient. Mass spectrometry was performed using Orbitrap Fusion™ Lumos Tribrid (Thermo Fisher Scientific). Proteomics data were analyzed using PEAKS Studio™ 8.5 (BSI).

Immunoblotting

Proteins were separated on Bolt 4–12% Bis-Tris protein gels (Thermo Fisher Scientific) and transferred onto a PVDF membrane (Thermo Fisher Scientific) following the manufacturer's instruc-tions. The membrane was blocked in 5% non-fat milk for 1 h and incubated for 18 h at 4°C with specific primary antibodies. Mem-branes were washed 6 times with TBST and incubated for 1 h at ambient temperature with respective secondary HRP-conjugated antibodies. Membranes were washed six times with TBST, and chemifluorescence signals were developed using a SuperSignal West Dura Extended Duration Substrate kit (Thermo Fisher Scientific) and documented on X-ray films.

Data availability

The original and normalized transcriptomics data are available in the Gene Expression Omnibus (GEO, GSE182706, https://www.ncbi.nlm.nih.gov/geo/query/acc.cgi?acc=GSE182706).

Expanded View for this article is available online.

Author contributions
Veronica I Shubayev: Conceptualization; Resources; Funding acquisition; Writing—review & editing. **Jennifer Dolkas:** Investigation; Methodology. **Glaucilene Ferreira Catroli:** Visualization; Methodology. **Andrei V Chernov:** Conceptualization; Data curation; Software; Formal analysis; Supervision; Vali-dation; Investigation; Visualization; Methodology; Writing - original draft; Pro-ject administration; Writing—review & editing.

In addition to the CRediT author contributions listed above, the contribu-tions in detail are:
VIS conceptualized the study, provided resources, designed the methodology (animal model), wrote, reviewed, and edited the manuscript, contributed to project administration, and acquired funding. JD investigated animal proce-dures and behavioral assays. GFC investigated animal procedures, behavioral assays, and analysis of the study. AVC conceptualized the study, designed the methodology (RNA-seq, affinity capture, and bioinformatics), contributed to the software, performed formal analysis and data curation, investigated and visualized the study, wrote the original draft, and wrote, reviewed, and edited the manuscript.

Disclosure and competing interests statement
The authors declare that they have no conflict of interest.

References

Adelmann M, Linington C (1992) Molecular mimicry and the autoimmune response to the peripheral nerve myelin P0 glycoprotein. *Neurochem Res* 17: 887–891

Ahmed MA, De Avila M, Polverini E, Bessonov K, Bamm VV, Harauz G (2012) Solution nuclear magnetic resonance structure and molecular dynamics simulations of a murine 18.5 kDa myelin basic protein segment (S72–S107) in association with dodecylphosphocholine micelles. *Biochemistry* 51: 7475–7487

Altschul SF, Koonin EV (1998) Iterated profile searches with PSI-BLAST—a tool for discovery in protein databases. *Trends Biochem Sci* 23: 444–447

Altschul SF, Madden TL, Schäffer AA, Zhang J, Zhang Z, Miller W, Lipman DJ (1997) Gapped BLAST and PSI-BLAST: a new generation of protein database search programs. *Nucleic Acids Res* 25: 3389–3402

Arbour N, Côté G, Lachance C, Tardieu M, Cashman NR, Talbot PJ (1999) Acute and persistent infection of human neural cell lines by human coronavirus OC43. *J Virol* 73: 3338–3350

Arbour N, Talbot PJ (1998) Persistent infection of neural cell lines by human coronaviruses. *Adv Exp Med Biol* 440: 575–581

Attal N, Jazat F, Kayser V, Guilbaud G (1990) Further evidence for 'pain-related' behaviours in a model of unilateral peripheral mononeuropathy. *Pain* 41: 235–251

Attal N, Martinez V, Bouhassira D (2021) Potential for increased prevalence of neuropathic pain after the COVID-19 pandemic. *Pain Rep* 6: e884

Benlarbi M, Laroche G, Fink C, Fu K, Mulloy RP, Phan A, Ariana A, Stewart CM, Prévost J, Beaudoin-Bussières G et al (2022) Identification of a SARS-CoV-2 host metalloproteinase-dependent entry pathway differentially used by SARS-CoV-2 and variants of concern Alpha, Delta, and Omicron. *bioRxiv* https://doi.org/10.1101/2022.02.19.481107 [PREPRINT]

Boggs JM (2006) Myelin basic protein: a multifunctional protein. *Cell Mol Life Sci* 63: 1945–1961

Boggs JM, Moscarello MA (1978) Structural organization of the human myelin membrane. *Biochim Biophys Acta* 515: 1–21

Bolger AM, Lohse M, Usadel B (2014) Trimmomatic: a flexible trimmer for Illumina sequence data. *Bioinformatics* 30: 2114–2120

Boziki MK, Mentis AA, Shumilina M, Makshakov G, Evdoshenko E, Grigoriadis N (2020) COVID-19 Immunopathology and the central nervous system: implication for multiple sclerosis and other autoimmune diseases with associated demyelination. *Brain Sci* 10: 345

Burks JS, DeVald BL, Jankovsky LD, Gerdes JC (1980) Two coronaviruses isolated from central nervous system tissue of two multiple sclerosis patients. *Science* 209: 933–934

Chattopadhyay S, Myers RR, Janes J, Shubayev V (2007) Cytokine regulation of MMP-9 in peripheral glia: implications for pathological processes and pain in injured nerve. *Brain Behav Immun* 21: 561–568

Chernov AV, Hullugundi SK, Eddinger KA, Dolkas J, Remacle AG, Angert M, James BP, Yaksh TL, Strongin AY, Shubayev VI (2020) A myelin basic protein fragment induces sexually dimorphic transcriptome signatures of neuropathic pain in mice. *J Biol Chem* 295: 10807–10821

Chernov AV, Remacle AG, Hullugundi SK, Cieplak P, Angert M, Dolkas J, Shubayev VI, Strongin AY (2018) Amino acid sequence conservation of the algesic fragment of myelin basic protein is required for its interaction with CDK5 and function in pain. *FEBS J* 285: 3485–3502

Clausen MV, Hilbers F, Poulsen H (2017) The structure and function of the Na, K-ATPase isoforms in health and disease. *Front Physiol* 8: 371

Cook SD, Dowling PC (1980) Multiple sclerosis and viruses: an overview. *Neurology* 30: 80–91

Croxford JL, Olson JK, Anger HA, Miller SD (2005) Initiation and exacerbation of autoimmune demyelination of the central nervous system via virus-induced molecular mimicry: implications for the pathogenesis of multiple sclerosis. *J Virol* 79: 8581–8590

Dahm T, Rudolph H, Schwerk C, Schroten H, Tenenbaum T (2016) Neuroinvasion and inflammation in viral central nervous system infections. *Mediators Inflamm* 2016: 8562805

Dubé M, Le Coupanec A, Wong AHM, Rini JM, Desforges M, Talbot PJ (2018) Axonal transport enables neuron-to-neuron propagation of human coronavirus OC43. *J Virol* 92: e00404-18

Edwards JA, Denis F, Talbot PJ (2000) Activation of glial cells by human coronavirus OC43 infection. *J Neuroimmunol* 108: 73–81

Ermis U, Rust MI, Bungenberg J, Costa A, Dreher M, Balfanz P, Marx G, Wiesmann M, Reetz K, Tauber SC *et al* (2021) Neurological symptoms in COVID-19: a cross-sectional monocentric study of hospitalized patients. *Neurol Res Pract* 3: 17

Ewels P, Magnusson M, Lundin S, Käller M (2016) MultiQC: summarize analysis results for multiple tools and samples in a single report. *Bioinformatics* 32: 3047–3048

Getts DR, Chastain EM, Terry RL, Miller SD (2013) Virus infection, antiviral immunity, and autoimmunity. *Immunol Rev* 255: 197–209

Glass WG, Subbarao K, Murphy B, Murphy PM (2004) Mechanisms of host defense following severe acute respiratory syndrome-coronavirus (SARS-CoV) pulmonary infection of mice. *J Immunol* 173: 4030–4039

Gutiérrez-Ortiz C, Méndez-Guerrero A, Rodrigo-Rey S, San Pedro-Murillo E, Bermejo-Guerrero L, Gordo-Mañas R, de Aragón-Gómez F, Benito-León J (2020) Miller Fisher syndrome and polyneuritis cranialis in COVID-19. *Neurology* 95: e601–e605

Hong S, Remacle AG, Shiryaev SA, Choi W, Hullugundi SK, Dolkas J, Angert M, Nishihara T, Yaksh TL, Strongin AY *et al* (2017) Reciprocal relationship between membrane type 1 matrix metalloproteinase and the algesic peptides of myelin basic protein contributes to chronic neuropathic pain. *Brain Behav Immun* 60: 282–292

Jacomy H, Fragoso G, Almazan G, Mushynski WE, Talbot PJ (2006) Human coronavirus OC43 infection induces chronic encephalitis leading to disabilities in BALB/C mice. *Virology* 349: 335–346

Johnson RT (1999) Nervous system viruses. In *Encyclopedia of Virology*, Granoff A, Webster RG (eds), pp 1013–1020. Amsterdam: Elsevier

Julius D, Basbaum AI (2001) Molecular mechanisms of nociception. *Nature* 413: 203–210

Jumper J, Evans R, Pritzel A, Green T, Figurnov M, Ronneberger O, Tunyasuvunakool K, Bates R, Žídek A, Potapenko A *et al* (2021) Highly accurate protein structure prediction with AlphaFold. *Nature* 596: 583–589

Kadlubowski M, Hughes RA (1979) Identification of the neuritogen for experimental allergic neuritis. *Nature* 277: 140–141

Kemp HI, Corner E, Colvin LA (2020) Chronic pain after COVID-19: implications for rehabilitation. *Br J Anaesth* 125: 436–440

Kidd BL, Urban LA (2001) Mechanisms of inflammatory pain. *Br J Anaesth* 87: 3–11

Kilinc D, van de Pasch S, Doets AY, Jacobs BC, van Vliet J, Garssen MPJ (2020) Guillain-Barré syndrome after SARS-CoV-2 infection. *Eur J Neurol* 27: 1757–1758

Kim Y, Remacle AG, Chernov AV, Liu H, Shubayev I, Lai C, Dolkas J, Shiryaev SA, Golubkov VS, Mizisin AP *et al* (2012) The MMP-9/TIMP-1 axis controls the status of differentiation and function of myelin-forming Schwann cells in nerve regeneration. *PLoS One* 7: e33664

Ko JS, Eddinger KA, Angert M, Chernov AV, Dolkas J, Strongin AY, Yaksh TL, Shubayev VI (2016) Spinal activity of interleukin 6 mediates myelin basic protein-induced allodynia. *Brain Behav Immun* 56: 378–389

Kobayashi H, Chattopadhyay S, Kato K, Dolkas J, Kikuchi S, Myers RR, Shubayev VI (2008) MMPs initiate Schwann cell-mediated MBP degradation and mechanical nociception after nerve damage. *Mol Cell Neurosci* 39: 619–627

Koike H, Chiba A, Katsuno M (2021) Emerging infection, vaccination, and Guillain-Barré syndrome: a review. *Neurol Ther* 10: 523–537

Koralnik IJ, Tyler KL (2020) COVID-19: a global threat to the nervous system. *Ann Neurol* 88: 1–11

Krämer A, Green J, Pollard Jr J, Tugendreich S (2014) Causal analysis approaches in ingenuity pathway analysis. *Bioinformatics* 30: 523–530

Lanz TV, Brewer RC, Ho PP, Moon J-S, Jude KM, Fernandez D, Fernandes RA, Gomez AM, Nadj G-S, Bartley CM *et al* (2022) Clonally expanded B Cells in multiple sclerosis bind EBV EBNA1 and GlialCAM. *Nature* 603: 321–327

Liu H, Shiryaev SA, Chernov AV, Kim Y, Shubayev I, Remacle AG, Baranovskaya S, Golubkov VS, Strongin AY, Shubayev VI (2012) Immunodominant fragments of myelin basic protein initiate T cell-dependent pain. *J Neuroinflamm* 9: 119

Love MI, Huber W, Anders S (2014) Moderated estimation of fold change and dispersion for RNA-seq data with DESeq2. *Genome Biol* 15: 550

Love MI, Soneson C, Hickey PF, Johnson LK, Pierce NT, Shepherd L, Morgan M, Patro R (2020) Tximeta: reference sequence checksums for provenance identification in RNA-seq. *PLoS Comput Biol* 16: e1007664

Manji H, Carr AS, Brownlee WJ, Lunn MP (2020) Neurology in the time of COVID-19. *J Neurol Neurosurg Psychiatry* 91: 568–570

Mao L, Jin H, Wang M, Hu YU, Chen S, He Q, Chang J, Hong C, Zhou Y, Wang D *et al* (2020) Neurologic manifestations of hospitalized patients with coronavirus disease 2019 in Wuhan, China. *JAMA Neurol* 77: 683–690

Maximova OA, Sturdevant DE, Kash JC, Kanakabandi K, Xiao Y, Minai M, Moore IN, Taubenberger J, Martens C, Cohen JI et al (2021) Virus infection of the CNS disrupts the immune-neural-synaptic axis via induction of pleiotropic gene regulation of host responses. eLife 10: e62273

McFarland AJ, Yousuf MS, Shiers S, Price TJ (2021) Neurobiology of SARS-CoV-2 interactions with the peripheral nervous system: implications for COVID-19 and pain. Pain Rep 6: e885

Mirdita M, Ovchinnikov S, Steinegger M (2021) ColabFold – making protein folding accessible to all. bioRxiv https://doi.org/10.1101/2021.08.15.456425 [PREPRINT]

Montalvan V, Lee J, Bueso T, De Toledo J, Rivas K (2020) Neurological manifestations of COVID-19 and other coronavirus infections: a systematic review. Clin Neurol Neurosurg 194: 105921

Musse AA, Boggs JM, Harauz G (2006) Deimination of membrane-bound myelin basic protein in multiple sclerosis exposes an immunodominant epitope. Proc Natl Acad Sci USA 103: 4422–4427

Patil M, Belugin S, Mecklenburg J, Wangzhou A, Paige C, Barba-Escobedo PA, Boyd JT, Goffin V, Grattan D, Boehm U et al (2019) Prolactin regulates pain responses via a female-selective nociceptor-specific mechanism. iScience 20: 449–465

Patro R, Duggal G, Love MI, Irizarry RA, Kingsford C (2017) Salmon provides fast and bias-aware quantification of transcript expression. Nat Methods 14: 417–419

Paulson PE, Casey KL, Morrow TJ (2002) Long-term changes in behavior and regional cerebral blood flow associated with painful peripheral mononeuropathy in the rat. Pain 95: 31–40

Pelech SL (1995) Networking with proline-directed protein kinases implicated in tau phosphorylation. Neurobiol Aging 16: 247–256

Remacle AG, Hullugundi SK, Dolkas J, Angert M, Chernov AV, Strongin AY, Shubayev VI (2018a) Acute- and late-phase matrix metalloproteinase (MMP)-9 activity is comparable in female and male rats after peripheral nerve injury. J Neuroinflammation 15: 89

Remacle AG, Hullugundi SK, Dolkas J, Angert M, Cieplak P, Scott D, Chernov AV, Shubayev VI, Strongin AY (2018b) Interaction of the cryptic fragment of myelin basic protein with mitochondrial voltage-dependent anion-selective channel-1 affects cell energy metabolism. Biochem J 475: 2355–2376

Remacle AG, Kumar S, Motamedchaboki K, Cieplak P, Hullugundi S, Dolkas J, Shubayev VI, Strongin AY (2015) Matrix metalloproteinase (MMP) proteolysis of the extracellular loop of voltage-gated sodium channels and potential alterations in pain signaling. J Biol Chem 290: 22939–22944

Risso D, Ngai J, Speed TP, Dudoit S (2014) Normalization of RNA-seq data using factor analysis of control genes or samples. Nat Biotechnol 32: 896–902

Ritchie ME, Phipson B, Wu D, Hu Y, Law CW, Shi W, Smyth GK (2015) limma powers differential expression analyses for RNA-sequencing and microarray studies. Nucleic Acids Res 43: e47

Romoli M, Jelcic I, Bernard-Valnet R, García Azorín D, Mancinelli L, Akhvlediani T, Monaco S, Taba P, Sellner J (2020) A systematic review of neurological manifestations of SARS-CoV-2 infection: the devil is hidden in the details. Eur J Neurol 27: 1712–1726

Roos RP (1983) Viruses and demyelinating disease of the central nervous system. Neurol Clin 1: 681–700

Şahin T, Ayyildiz A, Gencer-Atalay K, Akgün C, Özdemir HM, Kuran B (2021) Pain symptoms in COVID-19. Am J Phys Med Rehabil 100: 307–312

Sancho-Saldaña A, Lambea-Gil Á, Liesa JLC, Caballo MRB, Garay MH, Celada DR, Serrano-Ponz M (2020) Guillain-Barré syndrome associated with leptomeningeal enhancement following SARS-CoV-2 infection. Clin Med (Lond) 20: e93–e94

Savarin C, Bergmann CC (2017) Viral-induced suppression of self-reactive T cells: Lessons from neurotropic coronavirus-induced demyelination. J Neuroimmunol 308: 12–16

Shenoda BB, Ramanathan S, Gupta R, Tian Y, Jean-Toussaint R, Alexander GM, Addya S, Somarowthu S, Sacan A, Ajit SK (2021) Xist attenuates acute inflammatory response by female cells. Cell Mol Life Sci 78: 299–316

Shiryaev SA, Remacle AG, Savinov AY, Chernov AV, Cieplak P, Radichev IA, Williams R, Shiryaeva TN, Gawlik K, Postnova TI et al (2009) Inflammatory proprotein convertase-matrix metalloproteinase proteolytic pathway in antigen-presenting cells as a step to autoimmune multiple sclerosis. J Biol Chem 284: 30615–30626

Shubayev VI, Angert M, Dolkas J, Campana WM, Palenscar K, Myers RR (2006) TNFalpha-induced MMP-9 promotes macrophage recruitment into injured peripheral nerve. Mol Cell Neurosci 31: 407–415

Shubayev VI, Strongin AY, Yaksh TL (2016) Role of myelin auto-antigens in pain: a female connection. Neural Regen Res 11: 890–891

Shubayev VI, Strongin AY, Yaksh TL (2018) Structural homology of myelin basic protein and muscarinic acetylcholine receptor: significance in the pathogenesis of complex regional pain syndrome. Mol Pain 14: 1744806918815005

St-Jean JR, Jacomy H, Desforges M, Vabret A, Freymuth F, Talbot PJ (2004) Human respiratory coronavirus OC43: genetic stability and neuroinvasion. J Virol 78: 8824–8834

Stohlman SA, Hinton DR (2001) Viral induced demyelination. Brain Pathol 11: 92–106

Suzuki R, Dickenson AH (2000) Neuropathic pain: nerves bursting with excitement. NeuroReport 11: R17–R21

Syrett CM, Paneru B, Sandoval-Heglund D, Wang J, Banerjee S, Sindhava V, Behrens EM, Atchison M, Anguera MC (2019) Altered X-chromosome inactivation in T cells may promote sex-biased autoimmune diseases. JCI Insight 4: e126751

Talbot PJ, Arnold D, Antel JP (2001) Virus-induced autoimmune reactions in the CNS. Curr Top Microbiol Immunol 253: 247–271

Talbot PJ, Ekandé S, Cashman NR, Mounir S, Stewart JN (1993) Neurotropism of human coronavirus 229E. Adv Exp Med Biol 342: 339–346

Tang W, Zhang L, Li Z (2021) Long noncoding RNA LOC100911498 is a novel regulator of neuropathic pain in rats. Brain Behav 11: e01966

Troyer EA, Kohn JN, Hong S (2020) Are we facing a crashing wave of neuropsychiatric sequelae of COVID-19? Neuropsychiatric symptoms and potential immunologic mechanisms. Brain Behav Immun 87: 34–39

Tunyasuvunakool K, Adler J, Wu Z, Green T, Zielinski M, Žídek A, Bridgland A, Cowie A, Meyer C, Laydon A et al (2021) Highly accurate protein structure prediction for the human proteome. Nature 596: 590–596

Wang F, Cai B, Li K-C, Hu X-Y, Lu Y-J, Wang Q, Bao L, Zhang X (2015) FXYD2, a γ subunit of Na+, K+-ATPase, maintains persistent mechanical allodynia induced by inflammation. Cell Res 25: 318–334

Wege H, Watanabe R, Koga M, Ter Meulen V (1983) Coronavirus JHM-induced demyelinating encephalomyelitis in rats: influence of immunity on the course of disease. Prog Brain Res 59: 221–231

Weise MJ, Carnegie PR (1988) An approach to searching protein sequences for superfamily relationships or chance similarities relevant to the molecular mimicry hypothesis: application to the basic proteins of myelin. J Neurochem 51: 1267–1273

Weiss SR, Hughes SA, Bonilla PJ, Turner JD, Leibowitz JL, Denison MR (1994) Coronavirus polyprotein processing. Arch Virol Suppl 9: 349–358

Widyadharma IPE, Sari N, Pradnyaswari KE, Yuwana KT, Adikarya I, Tertia C, Wijayanti IAS, Indrayani IAS, Utami DKI (2020) Pain as clinical

manifestations of COVID-19 infection and its management in the
pandemic era: a literature review. *Egypt J Neurol Psychiatr Neurosurg* 56:
121

Zhao H, Shen D, Zhou H, Liu J, Chen S (2020) Guillain-Barré syndrome
associated with SARS-CoV-2 infection: causality or coincidence? *Lancet
Neurol* 19: 383–384